applied sciences

MDPI

Article

Dilatancy Characteristics and Constitutive Modelling of the Unsaturated Soil Based on Changes in the Mass Water Content

Xiao Xu [1], Guoqing Cai [2,*], Zhaoyang Song [2], Jian Li [2], Chongbang Xu [1], Hualao Wang [1] and Chengang Zhao [2,3]

1 Bridge and Tunnel Research Center, Research Institute of Highway Ministry of Transport, Beijing 100088, China; 13115267@bjtu.edu.cn (X.X.); cb.xu@rioh.cn (C.X.); hl.wang@rioh.cn (H.W.)
2 Key Laboratory of Urban Underground Engineering of Ministry of Education, Beijing Jiaotong University, Beijing 100044, China; 16115299@bjtu.edu.cn (Z.S.); jianli@bjtu.edu.cn (J.L.); cgzhao@bjtu.edu.cn (C.Z.)
3 School of Civil Engineering, Guilin University of Technology, Guilin 541004, China
* Correspondence: guoqing.cai@bjtu.edu.cn; Tel.: +86-188-1026-2621

Abstract: Most soil mechanics theories are limited to strain hardening and shrinkage under high compressive stresses, and there are some shortcomings in the selection of suction or degree of saturation as the water content state varies in the constitutive models of unsaturated soil. Based on the triaxial shear tests of unsaturated compacted soil (a silt of high plasticity) with different water content and confining pressure (low-confining), a shear dilatancy model of unsaturated soil based on the mass water content is proposed in this paper. The influence of the water content on the shear deformation characteristics of the unsaturated soil is analysed. The stress–dilatancy relationship and the prediction equation of the minimum dilatancy rate of the unsaturated soil under different water content and different confining pressure are provided. Selecting the mass water content as the state variable, a constitutive model suitable for the dilatancy of unsaturated soil is established. The method of determining model parameters based on the mass water content is analysed. The applicability of the model is verified by comparisons between the predicted and experimental results.

Keywords: soil mechanics; unsaturated soil; mass water content; stress–dilatancy relationship; minimum dilatancy rate; constitutive modelling

Citation: Xu, X.; Cai, G.; Song, Z.; Li, J.; Xu, C.; Wang, H.; Zhao, C. Dilatancy Characteristics and Constitutive Modelling of the Unsaturated Soil Based on Changes in the Mass Water Content. *Appl. Sci.* **2021**, *11*, 4859. https://doi.org/10.3390/app11114859

Academic Editor: Fernando M. S. F. Marques

Received: 19 April 2021
Accepted: 20 May 2021
Published: 25 May 2021

1. Introduction

Existing theories of rock and soil mechanics majorly focus on the strength and deformation characteristics of soil under high compressive stresses. The descriptions of stresses and deformations during shearing are limited to strain hardening and shrinkage. However, the soil is often subjected to low stress and tensile stress in engineering problems [1–3], and the stresses and deformations during shearing often exhibit peaks and dilatancy. In such cases, the soil mechanics theories that are based on the effect of a high compressive stress will no longer be applicable. Thus, it is necessary to establish an appropriate stress–strain relationship model to describe the actual working conditions with an improved accuracy.

The soils that are involved in geotechnical engineering practice are mostly overconsolidated or compacted unsaturated soils [4]. Presently, the main research ideas on the stress–strain relationship of unsaturated soils—starting from the Barcelona basic model (BBM) proposed by Alonso et al. [5]—which are mostly based on the critical state theoretical framework, can be unified as the Cambridge-type model. It is generally challenging to accurately describe the high peak stress ratio and dilatancy behaviour of the soil using this type of model, and the research on an appropriate stress–strain model is still lacking.

An appropriate dilatancy prediction equation (stress–dilatancy relationship) is the key to establishing a stress–strain constitutive model of soil [6]. Initially, the researchers expressed the dilatancy rate as various functional relationships of the current effective stress ratio η' and the critical state friction constant M. An experimental comparison then revealed that the dilatancy equation should also consider the soil compaction state variables that reflect the influences of the void ratios or the confining pressures. In the past two decades, experimental studies on the mechanical properties of the unsaturated soils have shown that the dilatancy is also a function related to the change in the water content under the unsaturated state [7,8]. However, little attention has been paid to the stress–dilatancy relationship of the unsaturated soil, and the function of the saturated soil is mostly directly adopted when deriving the constitutive model.

To better describe the dilatancy characteristics of soil, researchers have introduced multi-mechanism models, such as the boundary surface model [9] and the sub-loading surface model [10], in which the prediction method of the minimum dilatancy rate during the shear deformation process was introduced. Initially, based on the summary of the experimental patterns, Bolton [11], as well as Jefferies and Shuttle [12], expressed the minimum dilatancy rate D_{min} through their newly defined state parameters (stress state and compacted state), I_{R} (relative dilatancy index), and ψ_{ct} (volume deformation state parameter), respectively, as follows.

$$D_{\mathrm{min}} = \alpha \cdot I_{\mathrm{R}} \quad (1)$$

and

$$D_{\mathrm{min}} = X \cdot \psi_{\mathrm{ct}} \quad (2)$$

where α and X represent the dilatancy coefficients under the corresponding state parameters (they can also be referred to as the minimum dilatancy coefficient). Moreover, the minimum dilatancy coefficient has been obtained as a function of the soil fabric, as demonstrated in previous studies [11–13]. The changes in the water content in unsaturated soil will induce changes in the soil fabric, such as the transition from a single-pore distribution to a dual-pore fabric under aggregation [14–16]. However, there are relatively few studies on the relationship between the minimum dilatancy rate and change in the water content.

At the same time, the multi-mechanism models of unsaturated soils that have been attempted to be established in recent years have mostly adopted either suction or degree of saturation as the state variable for the water content [14,17]. Degree of saturation couples the impacts of the compaction state (such as the void ratio or confining pressure) and water content state simultaneously. Experimental studies have shown that the impact paths of the compaction state and water content state on the dilatancy of the soil are different, or even the opposite. Thus, they should be distinguished in the description. In addition, it is complicated to obtain the suction of the soil at the engineering site. The suction is often high when the soil is dry (specifically when the adsorption effect is dominant) [18], which could reach tens or even hundreds of MPa. In this case, it will no longer be applicable to use suction to characterise the water content state in the constitutive model.

Based on triaxial shear tests of the unsaturated compacted soils with different water contents and different confining pressures (low-confining), the variation in shear deformation characteristics of the unsaturated soils under different water contents and different compaction states, as well as the expression of the stress–dilatancy relationship, are explored in this study. The prediction equation of the minimum dilatancy rate based on the compaction state and mass water content during the shear process is provided. A constitutive model suitable for describing the shear deformation characteristics of the unsaturated compacted soil is established based on the mass water content. The model can properly simulate the peak stress and dilatancy characteristics of the unsaturated compacted soils with different water contents and confining pressures.

2. Material and Experimentation

2.1. Materials

In this study, the test soil sample was prepared artificially by mixing commercial kaolin and river sand at a dry weight ratio of 70 and 30%, respectively. The prepared soil that was obtained using this method contains rich clay minerals. The kaolin has a high purity (over 96%), a uniform grain-size distribution, an average grain size of approximately

20.3 μm, and stable properties and structures. In addition, the clay mineral composition in the soil sample is kaolin. As there are no expansive minerals, the influence of expansiveness can be neglected. Figure 1 illustrates the grain–size distribution of sand. Due to the high liquid limit of pure kaolin, the diffusion of water is relatively slow. Therefore, river sand is mixed to achieve an improvement, which is a common approach in engineering practices. The selection of this prepared soil can ensure a suitable repeatability and representativeness of the tests. Test material is classified as a silt of high plasticity or MH according to the Unified Soil Classification System (USCS). The physical properties of the tested soil are summarised in Table 1.

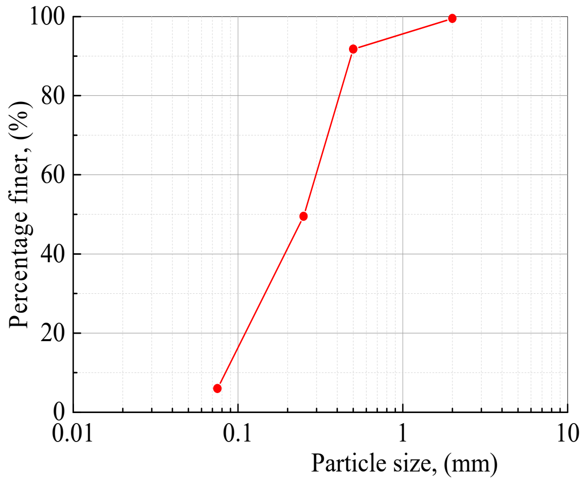

Figure 1. Grain-size distribution of sand.

Table 1. Physical properties of the tested soil.

Property Index	Value
Specific gravity	2.72
Liquid limit (%)	57
Plastic limit (%)	38
Plasticity index	19
Maximum dry density (g/cm^3)	1.3
Optimum water content (%)	36

2.2. Triaxial Test under Low Confining Pressures

In the test, the dry density of the soil sample is controlled at 1.2 g/cm^3, and the water contents is set at 4, 8, 12, 16, 20, 24, 28, 32, and 36%, respectively. Based on the soil water characteristic curve (SWCC) measured by the wetting contact filter paper method given in the Xiao et al. [18] test (used the same sample, shown in Figure 2, ρ_d in the figure represents the dry density of the sample), the suction of the samples in different water content states can be obtained [19]; the range of suction corresponding to the initial state of the specimen (sample preparation) is 86 to 8248 kPa (corresponding to the water content range from 36 to 4%). The triaxial samples with a diameter and height of 39.1 and 80.0 mm, respectively, are used, and the samples are prepared by implementing the layered compaction method. During the sample preparation process, the prepared wet soil samples with controlled water contents are measured according to the controlled dry density, and they are compacted in eight layers. Each layer is controlled to a height of 10 mm to ensure the uniformity of the sample. The triaxial shear test is conducted by applying GDS (Global Digital Systems Limited) unsaturated triaxial testing of soil (UNSAT), where the volume deformations of the samples are measured by the GDS-HKUST system (Global Digital Systems Limited—Hong Kong University of Science and Technology) [20]. During the test, a hard plastic film is used to separate the ceramic disk and sample to ensure that the test is performed under a constant water content. The top of the sample is connected to the atmosphere through the pore pressure control pipeline, and the pore-air pressure is maintained at 0 (relative atmospheric pressure) during the test. For the samples with different water contents, four sets of triaxial shear tests are performed under different confining pressures set to 0 (unconfined), 25, 50, and 100 kPa, respectively. To simulate the failure characteristics of the soils in a similar shallow environment under a constant water content, combined with the Xiao et al. [21] analysis, the confining pressure is applied at a rate of 25 kPa/20 min during the test. Once the confining pressure has reached the target value, it remains stable for 10 min to ensure that the pore-air pressure in the sample can be completely dissipated in time; that is, the compacted sample is fully consolidated and exhausted. Subsequently, the shear test is performed, and the shear rate is set to 0.1%/min during the test [21]. The shear test is terminated when the axial strain of the sample reaches 20%. After the shear test is completed, the sample is removed and its failure form can be observed. The mass change of the sample is weighed, and the water content of the sample is examined layer by layer. The error does not exceed 0.5%.

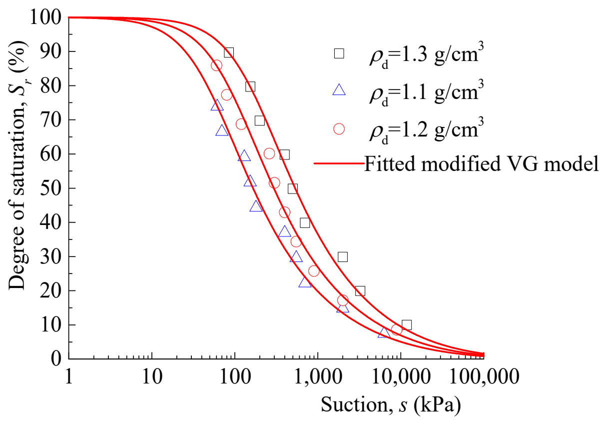

Figure 2. Soil-water characteristic curve.

Consolidated drained triaxial tests of the saturated samples are also conducted simultaneously for comparison. The dry density and water content are controlled at 1.2 g/cm^3 and 36%, respectively, to prepare the samples in the test. The sample preparation method is the same as that for the unsaturated triaxial test. The tests are performed after vacuum saturation and back pressure saturation. Compared with the unsaturated triaxial tests, two sets of higher confining pressures, 300 and 400 kPa, are added in the saturated state.

3. Test Results and Discussion

3.1. Shear Behaviours with Different Water Contents under Low Confining Pressures

The test results when the water content is 16% and the confining pressure is 50 kPa can be observed in Figure 3, which representatively illustrates the shear behaviours of the soil samples with different water contents during the triaxial test. Figure 3a shows the deviatoric stress; Figure 3b shows the volume strain; Figure 3c shows the variation of the stress ratio q/p in the shearing process with the dilatancy rate $d\varepsilon_v/d\varepsilon_d$. The following parameters are indicated in the figure: w is the water content of the sample (%), σ_3 is the confining pressure that is applied during the triaxial test, ε_1 is the axial strain during shearing, q is the deviatoric stress, p is the average net stress (the pore-air pressure is $u_a = 0$ during the test), ε_v is the volume strain, and ε_d is the deviatoric strain. During the triaxial test, the sample shows volume shrinkage in the beginning (point I in Figure 3 indicates the state point of maximum volume shrinkage), and then it transitions to dilatancy (point II corresponds to the peak stress state point). After passing the peak stress, the sample displays softening until the shearing stabilises. When the water content is high, sample softening is not evident. In a saturated state, the sample primarily shows shrinkage, shown in Figure 4 [22]. In this study, the development and change process of the stress and deformation during shearing are discussed.

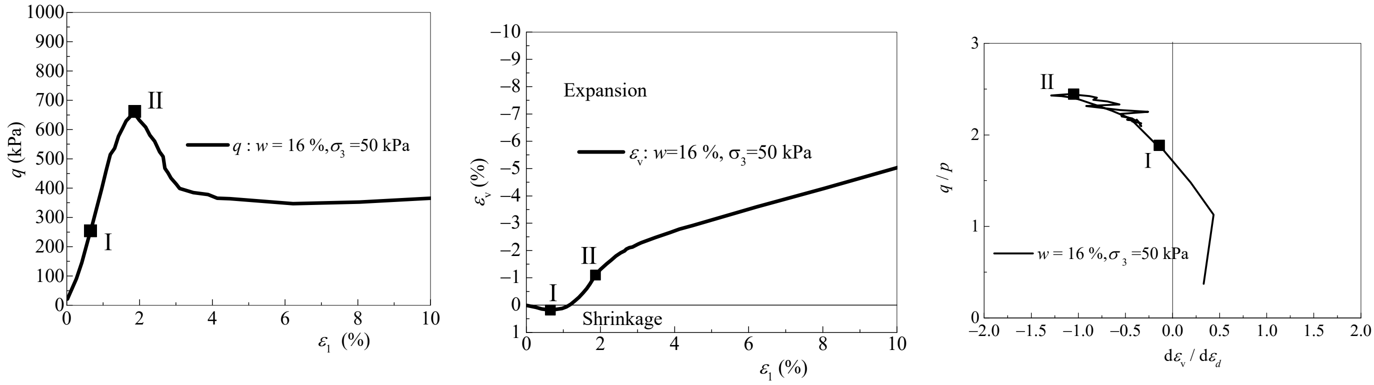

(**a**) (**b**) (**c**)

Figure 3. Shear behaviour of the triaxial tests: (**a**) deviatoric stress; (**b**) volume strain; (**c**) stress ratio with the dilatancy rate.

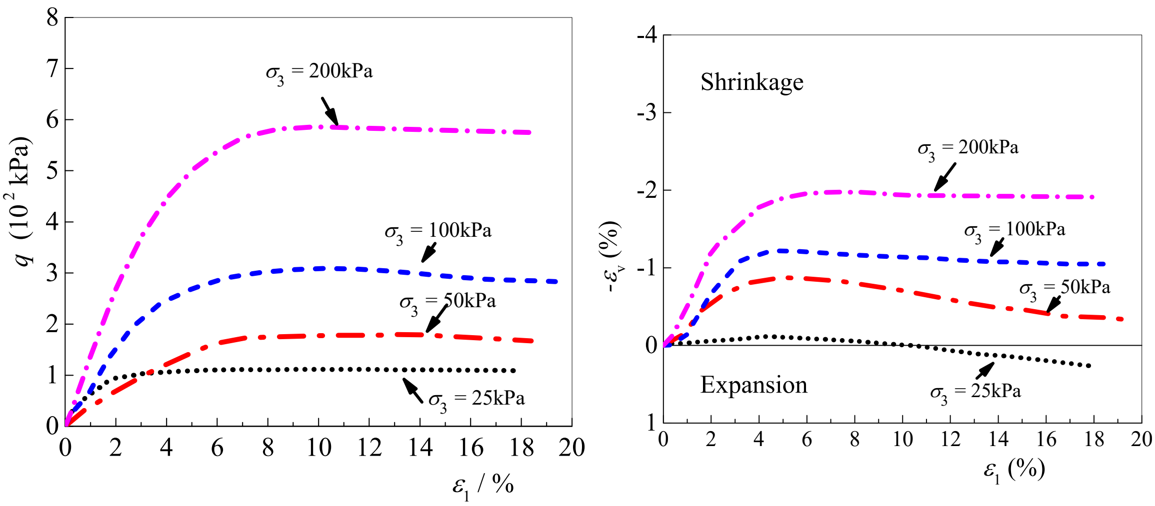

(**a**) Deviatoric stress (**b**) Volume strain

Figure 4. Shear behaviour at saturation.

3.2. Effective Stress between the Soil Particles in Unsaturated State

The effective stress between the unsaturated soil particles can be divided into external normal stress and inter-particle tensile stress caused by internal suction, which can be expressed using the average normal stress:

$$p' = p - \sigma^s \tag{3}$$

where p' denotes the effective stress in the unsaturated state; p can be directly obtained from the force that is applied on the sample surface. As for the inter-particle tensile stress σ^s (suction stress [23], negative), because the adsorption part is difficult to quantify, the uniaxial tensile strength σ_{tu} that is directly measured in the Xiao et al. [18] test (used the same sample, shown in Figure 5) is applied to approximate the σ^s ($\sigma_{\mathrm{tu}} = -\sigma^s$). Lu et al. [24] explained that this approximation method can be applied within a certain error range.

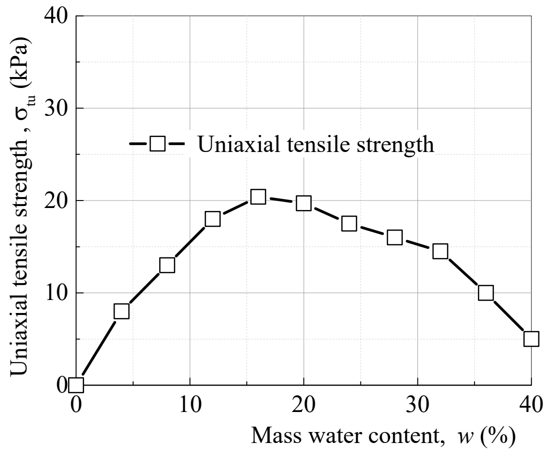

Figure 5. Tensile strength characteristic curve as a function of mass water content.

3.3. Change of the Sample State during the Shearing Process and the Shear Steady State

The tests showed that the water content has a significant impact on the shear deformation characteristics of the soils [25–27]. In the saturated state, the soil particles are dispersed and completely wrapped by water. During the shearing process, the particles are nearly sliding on the same plane, and there is almost no macroscopic volume change. As the water begins to drain, specifically when the water content falls below the plastic limit, the cohesive particles agglomerate, the pore-water shrinks and wraps in the agglomerate, or it forms a liquid meniscus at the contact point between the agglomerates. During the shearing process, the relatively large agglomerates or sand particles roll over each other, and the soil exhibits a relatively strong dilatancy macroscopically. The soil begins to exhibit properties of coarse-grained soils [28], such as when the water content is 36%. As the water content continues to decrease, this phenomenon tends to be more evident, such as when the water content is 16%. Thereafter that, as the water content continues to drop, the agglomerates begin to lose the adsorbed water and disperse. Subsequently, the agglomerates tend to return to the original grain size of kaolin (completely dried). In this case, the shear behaviour is similar to the fully saturated state; that is, the soil is sheared under its own particle size. However, because it is difficult to reach a completely dry state (water content of 0), the soil only exhibits characteristics that approximate the saturated state, such as when the water content is 4%.

During the shearing process, the mass water content of the soil remains unchanged, but the compaction state (specific volume) continues to change. Figure 6 shows the changing processes of the sample states on the $e - \ln p'$ plane during the shearing process at three water contents of 4, 16, and 36%, in which e represents the void ratio of the sample. The control state points of the shearing process are clearly labelled in the figure: the maximum volume shrinkage state point, namely the phase transition state point; the peak state point, namely the maximum deviatoric stress point; and the strain localisation state point, which can be referred to as the shear steady state point. At the shear steady state point, an obvious shear plane is formed, and the shearing of the sample tends to be stable. In other words, the stress tends to be constant, and the deformation continues to steadily develop. By comparing with the critical state definition, changes in the sample states during shearing indicate that the shear development is approaching the critical state. However, due to the occurrence of strain localisation, the sample deformation does not meet the critical state in the end; instead, it reaches a shear steady state. Moreover, due to the non-uniformity of the sample deformation, it is difficult to reach the strict critical state in the test. The shear steady state is chosen herein to approximate the critical state.

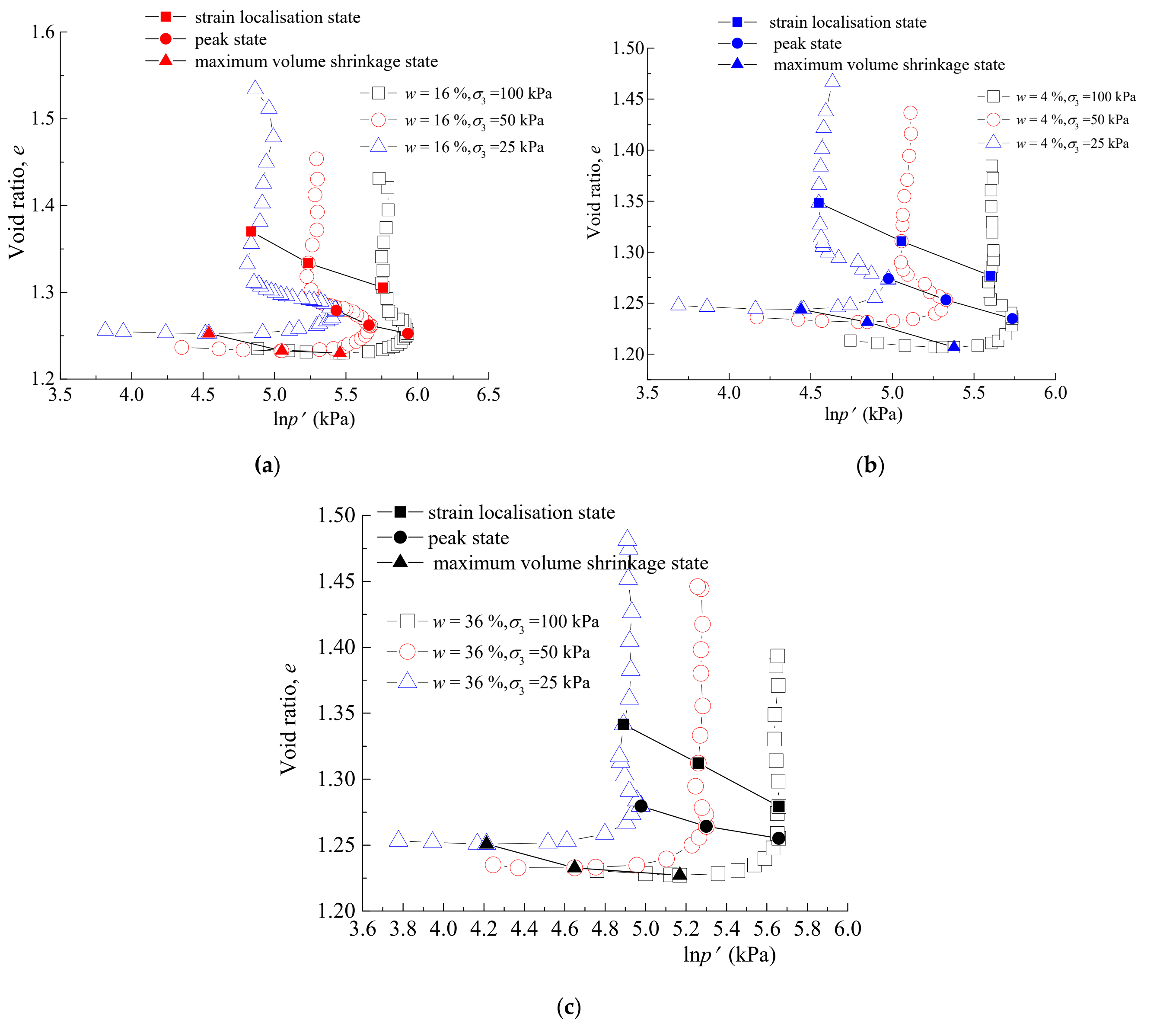

Figure 6. Sample state changes during shearing, w = : (**a**) 4%; (**b**) 16%; (**c**) 36%.

Figure 7 shows the critical state test points and the fitted critical state lines on q-p' and $e - \ln p'$ planes for the different mass water contents. The results show that the q-p' and $e - \ln p'$ relationships are almost parallel for the different mass water content states. Therefore, the critical state lines of the unsaturated soils with different mass water contents on the q-p' and $e - \ln p'$ planes have the same slopes of M and λ as the soil in the saturated state. The critical state lines of the unsaturated soils at the different mass water content states can be expressed as follows:

$$q = Mp' + \kappa(w) \tag{4}$$

$$e = \Gamma(w) - \lambda \ln p' \tag{5}$$

where M and $\kappa(w)$ represent the slope and intercept of the critical state line on the q-p' stress plane, respectively; and λ and $\Gamma(w)$ represent the slope and intercept of the critical state line of the soils with different water contents on the $e - \ln p'$ plane, respectively. Figure 7 lists the detailed parameters of the fitted critical state lines and correlation coefficients, from which it can be observed that the correlation coefficients are relatively high. In Figure 7b, the critical state line of the soil first moves upwards (saturated to 36, 16%) and then downwards (16 to 4%) with the decrease in the water content; this is due to the significant impact of the water content on the soil shear deformation characteristics that were previously mentioned.

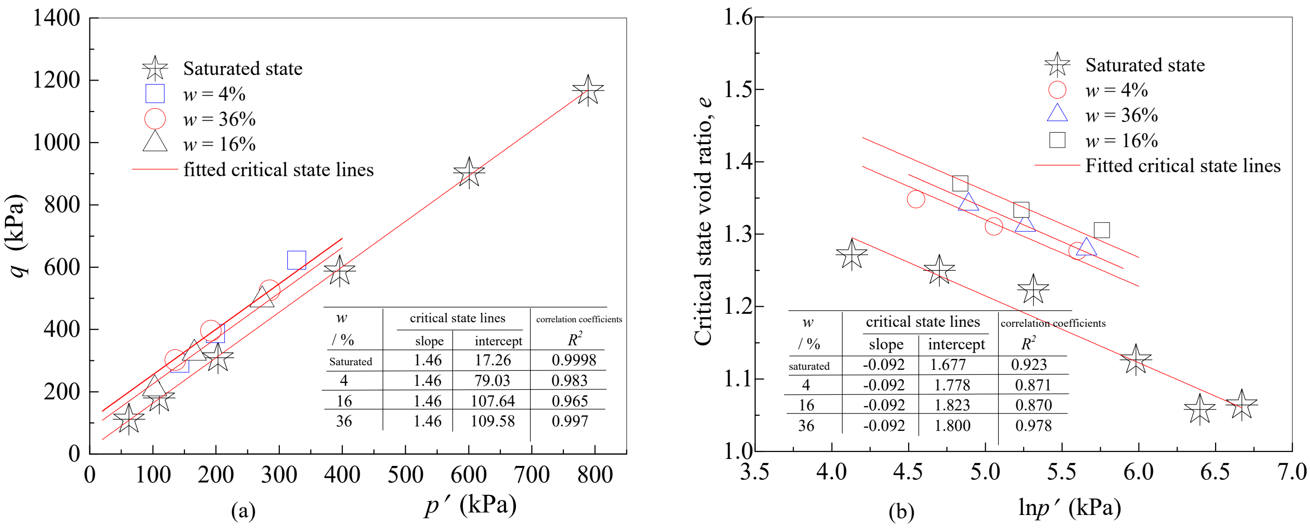

Figure 7. Critical state for the different water contents: (**a**) q-p'; (**b**) $e - \ln p'$.

3.4. Stress—Dilatancy Relationship

In the axisymmetric stress space of the triaxial test, the dilatancy rate can be expressed as $D = \mathrm{d}\varepsilon_{\mathrm{v}}^{\mathrm{p}}/\mathrm{d}\varepsilon_{\mathrm{d}}^{\mathrm{p}}$, where $\mathrm{d}\varepsilon_{\mathrm{v}}^{\mathrm{p}}$ and $\mathrm{d}\varepsilon_{\mathrm{d}}^{\mathrm{p}}$ represent the plastic volume strain increment and plastic deviatoric strain increment, respectively. The critical state theory shows that the peak strength of the soil can be described by two parts, the dilatancy and critical state strength; that is, it can be expressed as a stress–dilatancy equation. The triaxial test results in this study (Figure 3) show that the peak stress during shearing corresponds to the minimum dilatancy rate. Based on this observation, the relationship between η'_{max} and D_{min} is taken as the starting point to explore the stress–dilatancy equation of the unsaturated soils in the different volume states and water content states.

Figure 8 shows the relationships between the maximum effective stress ratio and minimum dilatancy rate for the varying water contents and confining pressures. It can be observed from the figure that η'_{max} and D_{min} approximate a linear relationship, which can be expressed as follows:

$$\eta'_{\mathrm{max}} = \eta_{\mathrm{r}} + \mu \cdot D_{\mathrm{min}} \tag{6}$$

where η_{r} and μ represent the friction and dilatancy parameters, respectively. In Figure 8, for the peak state, the representative fitted lines with the mass water contents of 4, 16, and 36% indicate that η_{r} remains unchanged at the critical state stress ratio M (same value for the saturated and unsaturated states) when the water content changes; moreover, μ is a function of the mass water content. In addition, at the same mass water content, the linear correlation of the test points under the different confining pressures implies that the value of μ is the same when the confining pressure changes. Therefore, the maximum effective stress ratio and minimum dilatancy rate in the unsaturated state develops along the same slope as the confining pressure changes, and the slope changes accordingly as the water content changes.

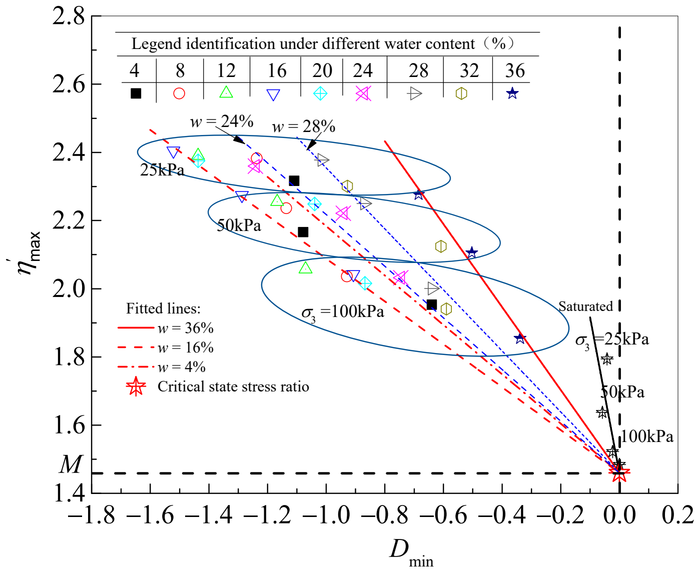

Figure 8. Relationship between the maximum effective stress ratio and minimum dilatancy rate.

Figures 9 and 10 demonstrate the relationships between the dilatancy rate and effective stress during shearing. Figure 9 shows the results when the water content is 4, 16, and 36% under the different confining pressures. At the same mass water content, the dilatancy rate–effective stress relationship can be approximated with the same straight line under the different confining pressures. In other words, the zero dilatancy rate point and the slope of the dilatancy rate change are the same. Figure 10 shows the results at a confining pressure of 25, 50, and 100 kPa under changing water contents, respectively. At the same confining pressure, the dilatancy rate can be observed to change approximately linearly with the effective stress along different slopes under the different water contents, and the zero dilatancy rate point can be approximated as the same.

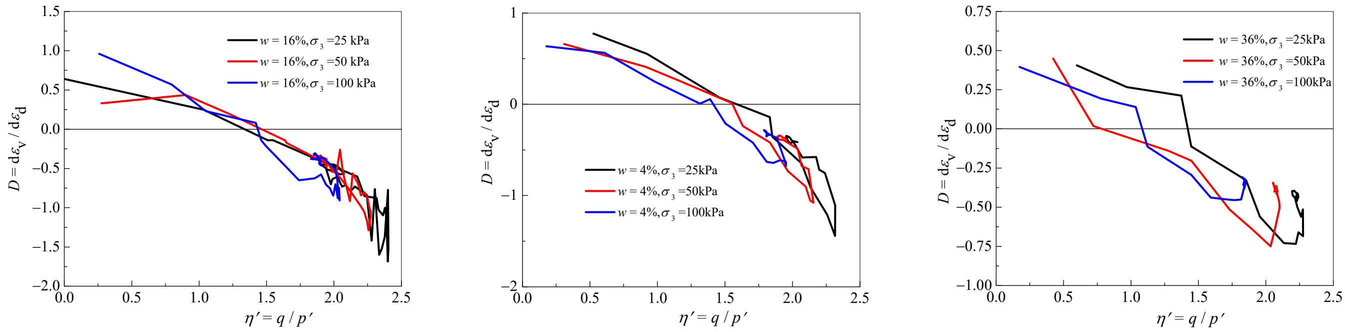

(**a**) (**b**) (**c**)

Figure 9. Relationship between the dilatancy rate and effective stress ratio for various confining stresses, w = : (**a**) 16%; (**b**) 4%; (**c**) 36%.

Based on the above analysis, under the different compaction states and water content states, the stress–dilatancy relationship for the unsaturated soil based on the mass water content can be expressed as follows:

$$D = \frac{M - \eta'}{-\mu(w)} \tag{7}$$

This is because the change in the water content state of the unsaturated soil has altered the soil fabric, thereby changing the slope of the change in the dilatancy rate with the current effective stress ratio. In other words, it changes the shear deformation characteristics of the soil. However, the compaction state only affects the amplitude of the dilatancy, but not the functional relationship of the dilatancy rate with the effective stress ratio. The above analysis indicates that the selection of the mass water content—a water content state parameter that decouples from the compaction state parameter—as the water content state variable can deliver a clear meaning and expression. Figure 11 shows the dilatancy parameters $\mu(w)$ for the different mass water contents that are obtained based on the test results.

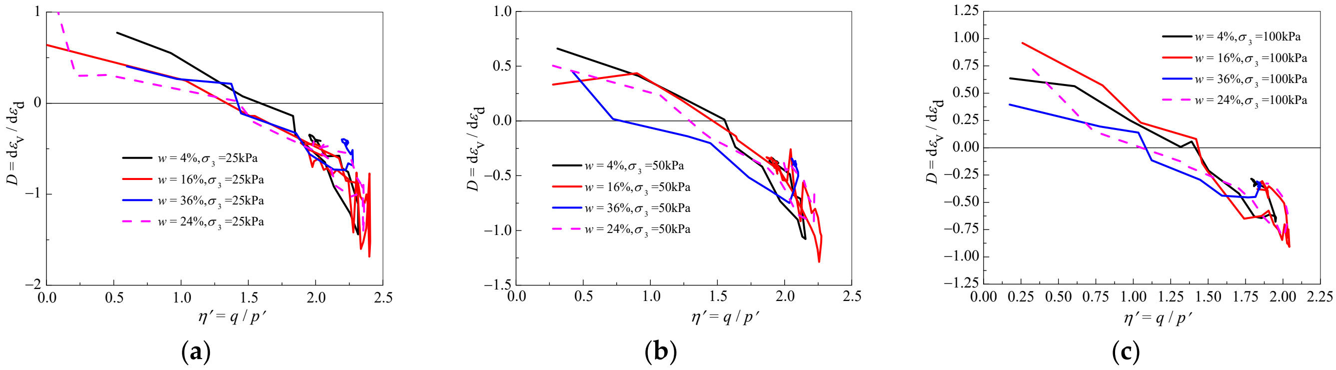

Figure 10. Relationship between the dilatancy rate and effective stress ratio for various water contents, σ_3 = : (**a**) 25 kPa; (**b**) 50 kPa; (**c**) 100 kPa.

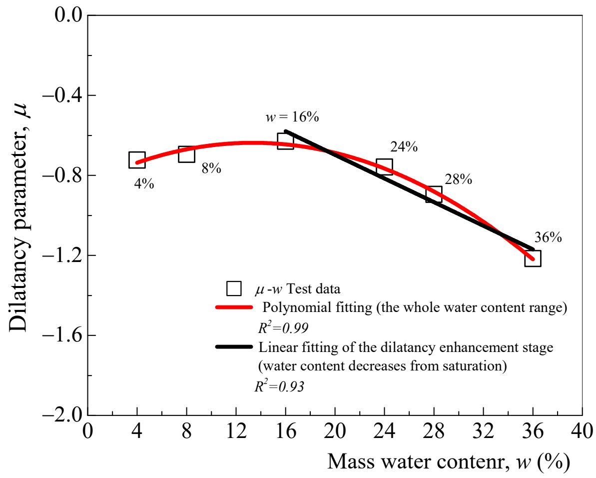

Figure 11. Relationship between the dilatancy parameter μ and mass water content w.

4. Constitutive Modelling

4.1. Yield Function and Compaction State Parameters

The above sections analysed the dilatancy characteristics of the unsaturated soils based on the mass water content. Accordingly, the constitutive model of the unsaturated soils with the different mass water contents during shearing can be established [29]. Based on the stress–dilatancy relationship (Equation (7)), the yield function can be expressed as follows:

$$F = \eta' - \frac{M}{1+\mu(w)}\left[1 + \mu(w)\cdot\left(\frac{p'}{p_{\mathrm{i}}}\right)^{(1+\mu(w))/-\mu(w)}\right] \tag{8}$$

where $\mu \neq -1$.

In this model, the image state points p_{i} (p_{i} represents the stress corresponding to the image state) are defined on each yield surface [30]; that is, the point on the yield surface where the plastic volume strain increment is zero. In addition, p_{i} is considered as the hardening parameter of the yield surface.

To consider the influence of the change of the compaction state (i.e., specific volume) during shearing in the model, the compaction state parameter based on the image state is defined as follows:

$$\psi_{\mathrm{i}} = e - e_{\mathrm{c,i}} \tag{9}$$

where $e_{\mathrm{c,i}}$ represents the void ratio on the critical state line corresponding to p_{i}.

4.2. Minimum Dilatancy Rate and State Parameters

By combining the compaction state parameter ψ_{i}, the minimum dilatancy rate of soil can be predicted, as shown in Figure 12, which leads to the following expression:

$$D_{\mathrm{min}} = X(w) \cdot \psi_{\mathrm{i}} \tag{10}$$

where $X(w)$ denotes the minimum dilatancy rate coefficient. By fitting the test results in Figure 12, the relationship between $X(w)$ and the mass water content can be obtained, as shown in Figure 13. The changing trend with the water content is consistent with the influence of the water content on the shear deformation characteristics of the soil that are described above.

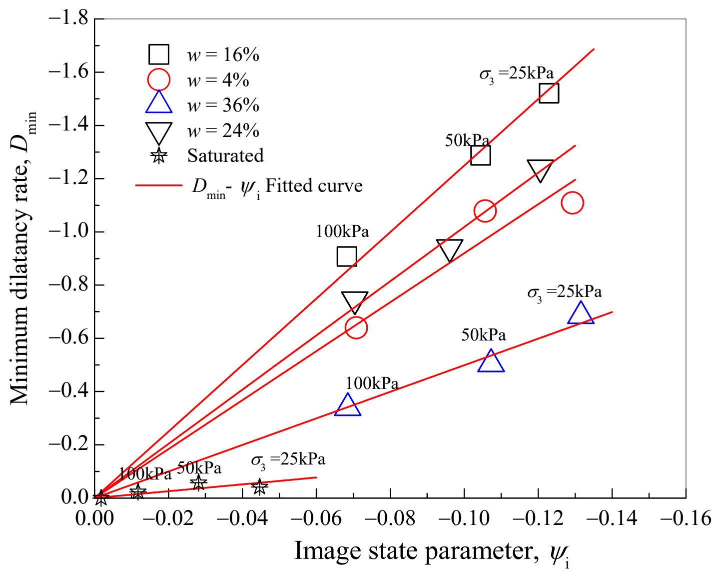

Figure 12. Minimum dilatancy rate and the corresponding state parameter ψ_{i}.

4.3. Maximum Yield Surface and Hardening Rule

Based on the minimum dilatancy rate, the maximum yield surface can be expressed as follows:

$$\frac{p_{\mathrm{i,max}}}{p'} = \left(1 + D_{\mathrm{min}} \cdot \frac{1+\mu(w)}{M}\right)^{\frac{\mu(w)}{1+\mu(w)}} \tag{11}$$

where $p_{\mathrm{i,max}}$ denotes the image stress that corresponds to the maximum yield surface, i.e., the maximum image stress.

The model assumes that the hardening and softening rate of the soil is a first-order function of the distance between the current state (expressed by the current image stress p_{i}) and the predictable peak state (expressed by $p_{\mathrm{i,max}}$), i.e., $(p_{\mathrm{i,max}} - p_{\mathrm{i}})$. Thus, the hardening rule can be expressed as follows [17]:

$$\frac{\dot{p}_{\mathrm{i}}}{\dot{\varepsilon}_{\mathrm{d}}^{\mathrm{p}}} = H \cdot M \exp\left(1 - \frac{\eta'}{M}\right) \cdot (p_{\mathrm{i,max}} - p_{\mathrm{i}}) \tag{12}$$

where $H = H_{\min} + \delta_H \psi_i$ represents the hardening modulus, $H_{\min}$ denotes the minimum hardening modulus, and δ_H is the variation coefficient based on the compaction state parameter.

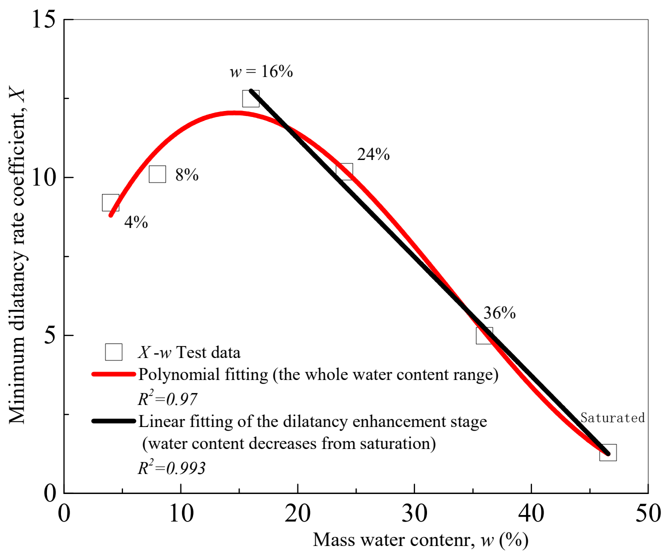

Figure 13. Relationship between the minimum dilatancy rate coefficient X and the mass water contents w.

4.4. Elastic Properties

The elastic properties are expressed as follows in the model [17]:

$$G = A\left(\frac{p'}{p_{\text{ref}}}\right)^n \tag{13}$$

$$K = \frac{2(1+v)}{3(1-2v)} \cdot G \tag{14}$$

where G is the elastic shear modulus, A is the shear modulus constant, n is the shear modulus exponent, p_{ref} is the unit reference pressure, K is the elastic bulk modulus, and v is Poisson's ratio.

4.5. Model Parameters

The current expression for the effective stress of the unsaturated soil cannot accurately describe the change in the contact stress between the soil particles that are caused by the physical and chemical effects [31,32]. Consequently, the inter-particle effective stress parameter σ^s of the unsaturated soil in the model can be preliminarily determined by applying the uniaxial tensile strength test.

Parameters M, λ, $\Gamma(w)$, $\mu(w)$, and $X(w)$ can be determined from the shear tests of the unsaturated soils with the different water contents. In addition, based on the accumulation of the test results, they can be provided directly based on the water content from the fitting relationships with the water content. As demonstrated by the tests in this study, the water content varies in a wide range, from saturated to almost completely dried, involving the whole moisture content variation range; the variations of the parameters $\Gamma(w)$, $\mu(w)$, and $X(w)$ exhibit a unimodal function form, which can be fitted with commonly used polynomials. For example, for the parameters $\mu(w)$ (Figure 11) and $X(w)$ (Figure 13), the following fitting functions can be obtained:

$$\mu = -1.14 \times 10^{-3} w^2 + 0.03w - 0.839 \tag{15}$$

$$X = 4.3 \times 10^{-4} w^3 - 0.043w^2 + 0.988w + 5.517 \tag{16}$$

When considering most of the currently available literature on unsaturated soil, engineering practice analyses, and some clays with a strong adsorption effect, the research on shear characteristics has mostly only involved (or been expressed in terms of) the enhancement of dilatancy from saturation to gradual water loss. That is, the stage where the parameter increases with the decrease in the water content. From the test results in this study, it can be observed that the dilatancy enhancement stage of the unsaturated soil—as the water content decreases from saturation—can be fitted with a relatively simple linear form. For example, the parameter $\mu(w)$ in Figure 11 and $X(w)$ in Figure 13 can be, respectively, fitted as follows:

$$\mu = -0.029w - 0.106 \tag{17}$$

$$X = -0.376w + 18.750 \tag{18}$$

This type of linear relationship is simpler, satisfying most requirements. The variation of the parameter $\Gamma(w)$ with the water content, as described in Section 3.3, exhibits similar characteristics as described above. In subsequent studies, by accumulating test results of the different soils, the model parameter prediction equation based on the water content can be further verified or provided, thus facilitating its promotion and application.

Parameters $H_{\min}$ and δ_H (i.e., hardening modulus H) can be obtained by fitting the deviatoric stress–strain curves in the triaxial tests (that is, trial calculation of the test results).

For the elastic parameters, A, n, and p_{ref} can be obtained from the unloading-reloading cycle test, and v can be obtained from the local deformation measurement test. In practice, the elastic deformation of the soil during shearing is negligible, and the total deformation can be considered as plastic deformation. Thus, the elastic deformation is neglected in the model calculation. However, starting from the theory, the elastic part is included to complete the model.

The initial condition for the calculation—that is, the void ratio e_0 of the sample before shearing—can be obtained from the volume deformation record during consolidating and air drainage by applying the confining pressures. Suction or degree of saturation is not directly introduced into the model; instead, the mass water content is used, which is more convenient for practical engineering applications.

5. Model Predictions

The capabilities of the proposed model are verified by using the triaxial shear tests of the unsaturated soils under different confining pressures and water contents. For the low-confining pressure triaxial tests performed in this study, the model calculation results and the test results are shown in Figure 14. Table 2 lists the model parameters and initial state parameters.

Table 2. Values of the model parameters and initial state parameters.

Mass Water Content w/%	Confining Pressure σ_3/kPa	Interparticle Tensile Stress σ^s/kPa		Initial Condition e_0	Critical State Line	
					λ	$\Gamma(w)$
4	25	−8		1.248	−0.092	1.778
16	100	−20.4		1.235	−0.092	1.823
36	50	−10		1.236	−0.092	1.800
Mass Water Content w/%	**Confining Pressure σ_3/kPa**	**Stress–Dilatancy Relationship**		**Dilatancy Coefficient $X(w)$**	**Hardening Modulus**	
		M	$\mu(w)$		$H_{\min}$	δ_H
4	25	1.460	−0.723	9.2	300	2
16	100	1.460	−0.629	12.49	140	2
36	50	1.460	−1.216	4.99	160	2

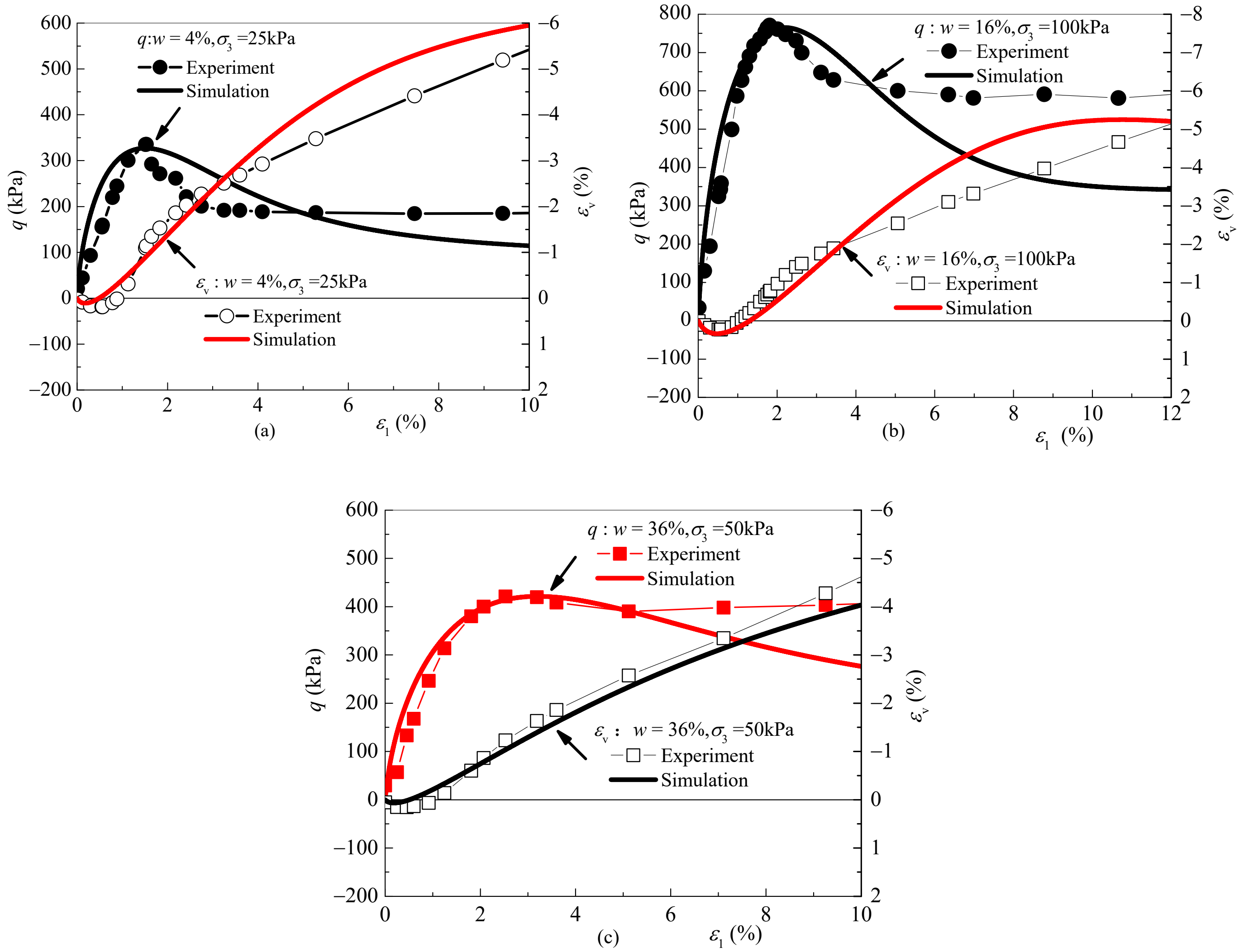

Figure 14. Comparison between the measured and computed results of the triaxial shear tests for the different confining pressures and water content of the unsaturated soil, (**a**) w = 4%, σ_3 = 25 kPa; (**b**) w = 16%, σ_3 = 100 kPa; (**c**) w = 36%, σ_3 = 50 kPa.

It can be observed that the proposed model can accurately simulate the hardening, maximum shrinkage state point, peak strength, and minimum dilatancy of the unsaturated compacted soils with different water contents and confining pressures. This is also the case for the soil strength and deformation, which are more concerned in practice. However, for soil softening and the subsequent strain localisation, the model calculation results are quite different from the test points. This is because the foundation of the model—namely the stress–dilatancy relationship and the critical state theoretical methods—are all based on the uniform deformation of the sample during shearing. The localisation of strain and the shear band phenomenon in the shear deformation process should be described by damage, bifurcation, and other special theories, which are not covered in this study.

6. Conclusions

(1) To decouple the effects of the water content state and compaction state and to facilitate engineering applications, the shear deformation characteristics of the unsaturated soils can be simulated based on the mass water content, thereby simplifying and clarifying the problem handling process;

(2) During the shearing process of unsaturated compacted soil under a low confining pressure, obvious dilatancy characteristics can be observed. The soil shows volume shrinkage in the beginning, and then transitions to dilatancy; after passing the peak stress, it displays softening until the shearing stabilises;
(3) The influence of the water content on the shear deformation characteristics of the unsaturated soils is analysed. The dilatancy characteristics show a unimodal changing pattern with the water content decreasing from saturation. As the water decreases, the soil particles disperse, agglomerate, and then deagglomerate; the dilatancy characteristics macroscopically first move upwards and then downwards;
(4) The stress–dilatancy relationship and the prediction equation of the minimum dilatancy rate of the unsaturated soil with different confining pressures and water contents are provided. From two aspects of the peak state point and the whole shear process, it is confirmed that the water content state alters the slope of the change, and the compaction state only affects the amplitude of the dilatancy in the effective stress ratio–dilatancy rate relationship. The minimum dilatancy rate can be directly predicted by the corresponding compaction state and water content state;
(5) By selecting the mass water content as the state variable, a constitutive model that is applicable to the dilatancy characteristics of the unsaturated soils is established. The methods for determining the model parameters based on the mass water content are analysed. Considering the stage where the parameter (or dilatancy) increases with the decrease in the water content, which is also the most concerned part of current engineering practice and academic research, the dilatancy parameters can be fitted with a relatively simple linear relationship. Based on the comparison between the triaxial shear test results and the calculation results under different confining pressures and different water contents, the applicability of the established model is verified.

Author Contributions: X.X. conceived and designed the experiments; X.X., G.C. and Z.S. performed the experiments; X.X., J.L. and C.X. analysed the data; H.W. and C.Z. did the analysis and discussion; X.X., G.C. and Z.S. did the modelling and wrote the paper. All authors have read and agreed to the published version of the manuscript.

Funding: This work was funded by the National Natural Science Foundation of China (grant number U2034204, 52078031, U1834206), Natural Science Foundation of Beijing (grant number 8202038), and Scientific Foundation of Shanxi Transportation Committee (grant number 2017-1-6).

Institutional Review Board Statement: Not applicable.

Informed Consent Statement: Not applicable.

Data Availability Statement: Not applicable.

Conflicts of Interest: The authors declare no conflict of interest.

References

1. Avila, F.; Puertas, E.; Gallego, R. Characterization of the mechanical and physical properties of unstabilized rammed earth: A review. *Constr. Build. Mater.* **2020**, *270*, 121435. [CrossRef]
2. Yin, P.; Vanapalli, S.K. Model for predicting the tensile strength of unsaturated cohesionless soils. *Can. Geotech. J.* **2018**, 55. [CrossRef]
3. Cai, G.; He, X.; Dong, L.; Liu, S.; Xu, Z.; Zhao, C.; Sheng, D. The shear and tensile strength of unsaturated soils by a grain-scale investigation. *Granular Matter* **2020**, *22*, 1. [CrossRef]
4. Gens, A. Soil-environment interactions in geotechnical engineering. *Géotechnique* **2010**, *60*, 3–74. [CrossRef]
5. Alonso, E.E.; Gens, A.; Josa, A. A constitutive model for partially saturated soils. *Géotechnique* **1990**, *40*, 405–430. [CrossRef]
6. Rivera-Hernandez, X.; Vahedifard, F.; Ellithy, G. Effect of suction and confining pressure on shear strength and dilatancy of highly compacted silty sand: Single-stage versus multistage triaxial testing. *Geotech. Test. J.* **2021**, 44.
7. Zhan, L.; Ng, C.W.W. Shear strength characteristics of an unsaturated expansive clay. *Can. Geotech. J.* **2006**, *43*, 751–763. [CrossRef]
8. Patil, U.D.; Hoyos, L.R.; Puppala, A.J.; Bheemasetti, T.V. Modeling stress-dilatancy behavior of compacted silty sand under suction-controlled axisymmetric shearing. *Geotech. Geol. Eng.* **2018**, *36*, 3961–3977. [CrossRef]

9. Dafalias, Y.F.; Herrmann, L.R. Bounding surface plasticity. II: Application to isotropic cohesive soils. *J. Eng. Mech.* **1986**, *112*, 1263–1291. [CrossRef]
10. Hashiguchi, K. Sub-loading surface model in unconventional plasticity. *Int. J. Solids Struct.* **1989**, *25*, 917–945. [CrossRef]
11. Bolton, M.D. The strength and dilatancy of sands. *Géotechnique* **1986**, *36*, 65–78. [CrossRef]
12. Jefferies, M.; Shuttle, D. Dilatancy in general Cambridge-type models. *Géotechnique* **2002**, *52*, 625–638. [CrossRef]
13. Jefferies, M.; Been, K. *Soil Liquefaction: A Critical State Approach*; Taylor & Francis: London, UK, 2006.
14. Patil, U.D.; Hoyos, L.R.; Morvan, M.; Puppala, A.J. Bounding surface-based modeling of compacted silty sand exhibiting suction dependent postpeak strain softening. *Int. J. Numer. Anal. Met.* **2018**, *42*, 1741–1761. [CrossRef]
15. Baker, R.; Frydman, S. Unsaturated soil mechanics: Critical review of physical foundations. *Eng. Geol.* **2009**, *106*, 26–39. [CrossRef]
16. Della, V.G.; Dieudonné, A.C.; Cristina, J.; Robert, C. Accounting for evolving pore size distribution in water retention models for compacted clays. *Int. J. Numer. Anal. Met.* **2015**, *39*, 702–723. [CrossRef]
17. Fern, E.J.; Robert, D.J.; Soga, K. Modeling the stress-dilatancy relationship of unsaturated silica sand in triaxial compression tests. *J. Geotech. Geoenviron.* **2016**, *142*, 04016055. [CrossRef]
18. Xu, X.; Cai, G.; Li, J.; Zhao, C. The strength and dilatancy characteristics of unsaturated soil at low and tensile stresses. *Chin. J. Rock Mech. Eng.* **2018**, *37*, 1933–1942.
19. Fredlund, D.G.; Sheng, D.C.; Zhao, J. Estimation of soil suction from the soil-water characteristic curve. *Can. Geotech. J.* **2011**, *48*, 186–198. [CrossRef]
20. Ng, C.W.W.; Zhan, L.T.; Cui, Y.J. A new simple system for measuring volume changes in unsaturated soils. *Can. Geotech. J.* **2002**, *39*, 757–764. [CrossRef]
21. Xu, X.; Zhao, C. Shear strength and volume change behavior of clay-rich soil at high suctions. *Rock Soil Mech.* **2018**, *39*, 1598–1610.
22. Xu, X.; Cai, G.; Li, J.; Zhao, C.; Zhao, C. Study on peak strength characteristics and failure envelope model of unsaturated soil. *Chin. J. Geotech. Eng.* **2020**, *7*, 1211–1219.
23. Lu, N.; Likos, W.J. Suction stress characteristic curve for unsaturated soil. *J. Geotech. Geoenviron.* **2006**, *132*, 13–142. [CrossRef]
24. Lu, N.; Kim, T.H.; Sture, S. Tensile strength of unsaturated sand. *J. Eng. Mech-Asce.* **2009**, *135*, 1410–1419. [CrossRef]
25. Romero, E.; Della, V.G.; Jommi, C. An insight into the water retention properties of compacted clayey soils. *Géotechnique* **2011**, *61*, 313–328. [CrossRef]
26. Merchán, V.; Vaunat, J.; Romero, E. *Drying Induced Effects on the Residual Strength of Remoulded Clays*; 3rd International Workshop on Unsaturated Soils; Taylor & Francis: Trento, Italy, 2009.
27. Toll, D.G. The Influence of Fabric on the Shear Behaviour of Unsaturated Compacted Soils. *Geo-Denver* **2000**, 222–234. [CrossRef]
28. Alonso, E.E.; Iturralde, E.F.O.; Romero, E.E. Dilatancy of Coarse Granular Aggregates. *Springer Proc. Phys.* **2007**, *112*, 119–135.
29. Cui, Y.J.; Delage, P. Yielding and plastic behaviour of an unsaturated compacted silt. *Géotechinique* **1996**, *46*, 291–311. [CrossRef]
30. Jefferies, M. Nor-Sand: A simple critical state model for sand. *Géotechnique* **1993**, *43*, 91–103. [CrossRef]
31. Lu, N.; Godt, J.W.; Wu, D.T. A closed-form equation for effective stress in unsaturated soil. *Water Resour. Res.* **2010**, *46*, 1–14. [CrossRef]
32. Zhao, C.G.; Liu, Z.Z.; Cai, G.Q. The principle of effective stress in unsaturated soil mechanics and its limitations. In Proceedings of the 6th International Conference on Unsaturated Soils (UNSAT), Sydney, Australia, 2–4 July 2014.